Tracer Mixing Dynamics During Aggregation and Fragmentation

Benjamin J. McCoy
Dept. of Chemical Engineering and Materials Science, University of California, Davis, CA 95616

Giridhar Madras
Dept. of Chemical Engineering, Indian Institute of Science, Bangalore 560 012, India

For many chemical systems consisting of particles, liquid droplets, or gas bubbles undergoing concurrent (reversible) aggregation and fragmentation in a stirred immiscible fluid, evolution of the particle distribution and mixing of chemical species are important fundamental issues. A dynamic model for dispersive mixing systems presented here illustrates the time dependence of the particle-size distribution (PSD) and the tracer mass distribution (TMD). For rapid tracer diffusion, the population balance equations (PBEs) for the PSD and TMD are identical (only the initial conditions differ) for binary aggregation and fragmentation rate coefficients that do not depend on particle size or tracer mass. The integrodifferential PBE is solved by a numerical method, and results agree with the moment solution. Measures for the degree of tracer mixing are related to the variance or polydispersity index and to the mixing entropy. The kinetics are reversible, allowing the PSD, TMD, and mixing entropy to approach stationary states. Results are partially compared with a similarity solution for the PSD.

Introduction

When agglomerating particles, liquid droplets, or gas bubbles are mixed in a stirred immiscible fluid, they generally undergo concurrent breakup (fragmentation) and aggregation (coalescence). An initial size distribution of such particles, droplets or bubbles, henceforth, generically called particles, will evolve to a steady-state particle-size distribution (PSD) that depends on the properties of the system, and in particular, on the breakage and coalescence rates. The central issue is to determine the PSD as a function of time, given the properties of the system and an initial condition for the PSD. The zeroth, first, and second moments of the PSD provide the number of particles, their mass, and their number- or mass-average size as functions of time. Particle breakage and coalescence events are governed by rate and stoichiometric coefficients based on binary processes. Thus, two particles are combined by aggregation, and two daughter particles are formed by fragmentation. The time evolution and final stationary state will depend on the energy input and turbulence energy spectrum (as determined, for example, by impeller speed), fluid properties (viscosities, interfacial energies), and mixer geometry (dimensions of vessel, impeller, and baffles). These influences are assumed to be embodied in the breakage and coalescence rate coefficients.

A chemical species, or tracer, concentrated in an initial fraction of the particles will become dispersed among the continuously forming new particles as the tracer is transferred from one into two particles by binary fission (breakup), and is combined from two particles into one by binary fusion (coalescence). We assume that the breakage rate is slower than the time for the tracer to diffuse throughout a new particle formed by aggregation of two particles having a different tracer concentration; thus, the tracer in an aggregated particle will be uniform prior to particle fragmentation. This resembles but simplifies a mixing process based on stretching and folding of stratified layers (Ottino et al., 1992). The process incorporates alternating separation and contacting, which are analogous to breakup and coalescence, respectively. If the particles are immersed in a well-stirred (turbulent) fluid medium, the particles are dispersed randomly throughout the medium, thereby manifesting temporal but not spatial dependence.

Correspondence concerning this article should be addressed to B. J. McCoy at this current address: Dept. of Chemical Engineering, Louisiana State University, Baton Rouge, LA 70803.

In a perspective on modeling the hydrodynamics of multiphase flow reactors, Sundaresan (2000) stressed the importance of fluid–solid, gas–liquid, and liquid–liquid interactions, and referred to the challenges in treating coalescence and breakup. In any mixing process, the rate mechanism is necessary to calculate the time required to mix materials under different conditions (Weidenbaum, 1958). Valentas and Amundson (1966) were among the first to model mathematically the breakage and coalescence of droplets, and their model was applied to steady-state drop-size distributions (Chatzi and Kiparissides, 1995). Coulaloglou and Tavlarides (1977) proposed models for agitated liquid–liquid dispersions that described the effect of impeller speed on maximum stable drop size for drops greater than the turbulence microscale. A tracer method to acertain a degree of mixing among dispersed particles was introduced by Church and Shinnar (1961). Prince and Blanch (1990) described experiments and a Monte Carlo theory for turbulent gas–liquid dispersions. Tracer gases in the bubbles were used to measure coalescence and breakage events. To model the degree of breakup, the theory was based on an assumed maximum stable size for bubbles. Tracer methods also have been used successfully in precipitation (Ilievski and White, 1995) and granulation (Pearson et al., 2001) experiments. Hounslow et al. (2001) provided a general population balance approach that is consistent with the present work, as we explain below. Ramkrishna (2000) recently reviewed theory and applications of population balances to particulate systems, emphasizing similarity behavior.

Madras and McCoy (2002) demonstrated how PBEs incorporating both fragmentation and aggregation can be solved numerically for general power-law size-dependent rate coefficients and arbitrary stoichiometric coefficients. Solutions for such reversible PBEs were shown to evolve to unique stationary states that approximated self-similar distributions in many cases. Earlier, an exact similarity solution was provided for the reversible random-fission PBE when the fragmentation rate coefficient was proportional to particle mass (McCoy and Madras, 1998). The midpoint-fission PBE provided a similarity solution for the first three moments, but not for the complete distribution. Whereas most discussions of similarity solutions have been restricted to irreversible fragmentation (Goren, 1968; Spicer and Pratsinis, 1996; Ziff, 1991; Ramkrishna, 2000; Muzzio et al., 1991; Kostoglou and Karabelas, 2001; Ottino et al., 1992), or irreversible aggregation (Cohen, 1992; Aizenman and Bak, 1979; Friedlander and Wang, 1966; Family et al., 1986), the more general theory takes on the reversible case. Of course, the irreversible special cases must be retrievable as limits of the general reversible model.

The concept of a maximum stable particle size has influenced modeling efforts for liquid–liquid dispersions (Kostoglou and Karabelas, 2001) and has been used to bolster the irreversible theory. In essence the turbulence spectrum is assumed to have a limiting energy level so that droplets smaller that the maximum stable size cannot be broken. In fact, however, the turbulence spectrum is not sharply bounded, and fluctuations of a broad energy distribution should be expected (Lam et al., 1996). Moreover, according to the irreversible notion, breakage always dominates when droplets are dilute, so that coalescence need not be accounted. This assumption becomes less applicable when the particle concentration increases with time in fragmentation-dominated systems, and the probability of coalescence, being second-order in concentration, increases. Ottino et al. (2000) suggested that for dispersed phase-volume fractions above 0.005, coalescence can be important. In our view, as time increases to large values, the coalescence rate becomes comparable to the fragmentation rate, and should not be ignored as the dynamic reversible stationary state is approached. Concern was expressed (Kostoglou and Karabelas, 2001) about the quantitative determination of the maximum stable drop size, because of the perception that steady state may not be attainable during practical experimental time periods. Experiments were cited to show that measured maximum drop size continued to decrease over very long mixing times. It was also suggested that observation of self-similarity for drop-size distributions was incompatible with a maximum stable drop size. Here we treat the case when the stable particle size is negligibly small. Appreciable minimum particle sizes can be handled similarly to minimum-MW oligomer products in macromolecular degradation (Madras and McCoy, 2001).

The neglect of coalescence is valid when the system is specifically stabilized, for example, by adding protective colloids (Church and Shinnar, 1961). For experiments with unstabilized droplets, a straightforward test for coalescence is to add some dyed drops to the distribution. If all or a large number of drops are dyed after a time, then coalescence must have occurred to cause the observed mixing. Church and Shinnar (1961), reporting such an experiment in an unstabilized liquid–liquid dispersion, found that intermixing was complete within minutes. In principle, the rate of mixing in the particles provides information about the relative effects of fragmentation and coalescence. The mathematical understanding of such mixing, needed for quantitative interpretation of the experiments, has not been conclusively resolved.

The goal of the current work is to determine the evolution in time of the PSD and the tracer mass distribution (TMD) from the given initial conditions to the final stationary states. More generally, reactant species will react with each other or diffuse out of particles and react with components in the surrounding fluid medium. Although the inert-species mixing problem addressed here lumps the detailed physics into the fragmentation and aggregation rate parameters, it has the advantage that it can be completely solved for various initial and rate conditions, evolves realistically in time, and, thus, can provide insights into general mixing processes beyond the specific problem considered.

We begin by writing the population balance equations for the PSD and for the TMD, and show how they can be solved in a dimensionless form. The moments of the PSD and TMD are quantities derived from the PBE solutions that relate to observable characteristics of physical systems. The solutions allow consideration of mixing entropy for both PSD and TMD. The PBEs have solutions that provide realistic results when the rate coefficients are independent of particle size. When the fragmentation rate coefficient is proportional to particle mass, and if the initial distribution is of an exponential form, the PBE obeys a similarity exponential solution throughout its evolution to steady state. This special solution permits particularly straightforward computations of observable moments and time-dependent entropy. Degrees of mixing are determined by comparison metrics for the PSD and

TMD, in particular how their variances or statistical entropy values are related.

Distribution Kinetics

We consider the PSD and TMD of the same particles. The PSD is defined so that $p(x,t)dx$ is the number of particles at time t in the mass range $(x, x + dx)$. If χ is the mass fraction of tracer in a particle, then $z = \chi x$ is the tracer mass in the particle. The TMD can be defined such that $c(z,t)dz$ is the number of particles at time t with tracer in the mass range $(z, z + dz)$. It follows that mass moments can be defined for $j = 0, 1, 2, \ldots$ as

$$p^{(j)}(t) = \int_0^\infty p(x,t)x^j \, dx \tag{1}$$

and

$$c^{(j)}(t) = \int_0^\infty c(z,t)z^j \, dz \tag{2}$$

The number of particles must be the same for the two distributions

$$p^{(0)}(t) = c^{(0)}(t) \tag{3}$$

The mass of particles, $p^{(1)}(t)$, and mass of tracer, $c^{(1)}(t)$, lead to the definition of average particle mass, $p^{\text{avg}}(t) = p^{(1)}(t)/p^{(0)}(t)$, and average tracer mass in the particles, $c^{\text{avg}}(t) = c^{(1)}(t)/c^{(0)}(t)$. Second moments provide measures of the PSD or TMD breadth, such as variance, $c^{\text{var}} = c^{(2)}/c^{(0)} - (c^{\text{avg}})^2$, or polydispersity, $c^{pd} = c^{(2)}c^{(0)}/c^{(1)2}$.

When fragmentation and aggregation are uncorrelated, the reversible binary processes can be represented as

$$P(x) \underset{k_a(x,x-x')}{\overset{k_b(x)}{\rightleftharpoons}} P(x') + P(x - x') \tag{4}$$

where $k_b(x)$ and $k_a(x, x - x')$ represent the rate coefficients for fragmentation (breakage) and aggregation, respectively. Recognizing that the tracer mass fraction, χ, is transported along with the particle mass, and assuming that the tracer does not affect the rates, we postulate a process similar to Eq. 4 for the tracer mass. Satisfying a mass balance as in Eq. 4, the process for tracer mass can, thus, be written as

$$C(z) \underset{k_a(x,x-x')}{\overset{k_b(x)}{\rightleftharpoons}} C(z') + C(z - z') \tag{5}$$

We assume the tracer mass is uniform throughout the particles by its high diffusivity (Hounslow et al., 2001), and is, thus, proportional to the particle mass. But the rate coefficients depend on particle mass, x, and not on tracer mass, z, as indicated in Eq. 5.

The governing PBE is first order for fission and second order for fusion (McCoy and Madras, 1998)

$$\begin{aligned} \partial p(x,t)/\partial t = &- k_b(x)p(x,t) \\ &+ 2\int_x^\infty k_b(x')p(x',t)\Omega(x,x') \, dx' \\ &- 2p(x,t)\int_0^\infty k_a(x,x')p(x',t) \, dx' \\ &+ \int_0^x k_a(x',x - x')p(x',t)p(x - x',t) \, dx' \end{aligned} \tag{6}$$

The PBE, Eq. 6, reduces to pure fragmentation or pure aggregation, respectively, when k_a or k_b vanish. The stoichiometric kernel, $\Omega(x,x')$, gives the product mass distribution for the binary fission and satisfies symmetry and normalization conditions, so $\Omega(x,x') = \Omega(z,z')$. McCoy and Wang (1994) proposed a general fragmentation stoichiometric kernel that can represent the entire range of product distributions from random to midpoint fission, $1/x'$ and $\delta(x - x'/2)$, respectively. For a well-stirred fluid the aggregation rate coefficient should be relatively independent of the masses of the coalescing particles, thus, in the present work we let $k_a(x', x - x') = k_a$, a constant. The breakage rate will increase with the size of the fragmenting particle in general, for example, as x^λ, but if we consider k_b constant ($\lambda = 0$), the issue of how k_b depends on x and/or on z is immaterial. Our assumption of mass-independent breakage coefficients is presented as a simplifying special case that permits quantitative analysis of issues that would be obscured by more complicated models. Hounslow et al. (2001) have recently provided a general PBE for a bivariate distribution of particle mass and tracer concentration. For rate coefficients independent of particle mass, the present balance equations for $p(x,t)$ and $c(z,t)$ can be obtained simply by integrating their PBE over z and x, respectively.

It is not only convenient but instructive mathematically to make the equations dimensionless. The rate coefficient, $k_b(x)$, requires that its x dependence be included in the scaling procedure. If one defines the reference rate coefficients for $x = p_o^{\text{avg}}$, such that $k_{bo} = k_b(x = p_o^{\text{avg}})$, then we can write the dimensionless quantities (Madras and McCoy, 2002)

$$\begin{aligned} \kappa(\xi) &= k_b(x)/k_{bo} \\ \gamma &= k_a p_o^{(0)}/k_{bo} \\ \theta &= tk_{bo} \end{aligned} \tag{7}$$

We scale the distributions with the initial quantities, $p_o^{(0)}$ and p_o^{avg}, as follows

$$\begin{aligned} \xi &= x/p_o^{\text{avg}} \\ P(\xi,\theta)d\xi &= p(x,t)dx/p_o^{(0)} \\ P(\xi,\theta) &= p(x,t)p_o^{\text{avg}}/p_o^{(0)} \\ P^{(n)}(\theta) &= p^{(n)}(t)/p_o^{(0)}p_o^{\text{avg}n} \\ \omega(\xi,\xi') &= \Omega(x,x')p_o^{\text{avg}} \end{aligned} \tag{8}$$

Similar nondimensional operations can be applied to $c(z,t)$

$$\zeta = z/c_o^{\text{avg}}$$

$$C(\zeta,\theta)d\zeta = c(z,t)dz/c_o^{(0)}$$

$$C(\zeta,\theta) = c(z,t)c_o^{\text{avg}}/c_o^{(0)}$$

$$C^{(n)}(\theta) = c^{(n)}(t)/c_o^{(0)}c_o^{\text{avg}n}$$

$$\omega(\zeta,\zeta') = \Omega(z,z')c_o^{\text{avg}} \tag{9}$$

We multiply Eq. 6 by $p_o^{\text{avg}}/p_o^{(0)}k_{bo}$ and rearrange to obtain the dimensionless PBE

$$\partial P(\xi,\theta)/\partial\theta = -\kappa(\xi)P(\xi,\theta) + 2\int_{\xi}^{\infty}\kappa(\xi')P(\xi',\theta)\omega(\xi,\xi')\,d\xi' - 2P(\xi\theta)\gamma\int_0^{\infty}P(\xi',\theta)\,d\xi' + \gamma\int_0^{\xi}P(\xi',\theta)P(\xi-\xi',\theta)\,d\xi' \tag{10}$$

The jth moments for a scaled distribution $P(\xi,\theta)$ are defined as

$$P^{(j)}(\theta) = \int_0^{\infty}\xi^j P(\xi,\theta)\,d\xi \tag{11}$$

and similarly for the TMD. If $\kappa(\xi)$ is constant, then the PBE for the TMD is identical to Eq. 11 with $C(\zeta,\theta)$ replacing $P(\xi,\theta)$. More generally, we let $\kappa(\xi) = \xi^{\lambda}$ in the following. The moment operation is applied to Eq. 11 to give the moment equations (Madras and McCoy, 2002)

$$dP^{(j)}/d\theta = -P^{(j+\lambda)} + 2Z_{jm}P^{(j+\lambda)} - 2\gamma P^{(j+\lambda)}P^{(0)} + \gamma\sum_{d=0}^{j}\binom{j}{d}P^{(j-d)}P^{(d)} \tag{12}$$

where $\binom{j}{d}$ is the binomial coefficient and Z_{jm} is $1/(1+j)$ for random and $1/2^j$ for midpoint fission. The moment equations for $j = 0$, 1, and 2 are

$$dP^{(0)}/d\theta = P^{(\lambda)} - \gamma P^{(0)2} \tag{13}$$

$$dP^{(1)}/d\theta = 0 \tag{14}$$

$$dP^{(2)}/d\theta = -(1/\sigma)P^{(2+\lambda)} + 2\gamma P^{(1)2} \tag{15}$$

The fragmentation stoichiometry affects only the second moment through Eq. 15, where $\sigma = 3$ for random fission and 2 for midpoint fission. Equation 14 ensures that particle mass is constant with time.

The limiting case of $k_a = 0$ (fragmentation only) gives $\gamma = 0$, so that Eqs. 13–15 reduce to (McCoy and Madras, 1998)

$$dP^{(0)}/d\theta = P^{(\lambda)} \tag{16}$$

$$dP^{(1)}/d\theta = 0 \tag{17}$$

$$dP^{(2)}/d\theta = -(1/\sigma)P^{(2+\lambda)} \tag{18}$$

When $\lambda > 0$, there is no closure for the second moment, Eq. 18. When no fragmentation occurs, we set $k_{bo} = 0$, so that Eqs. 13–15 reduce to

$$dP^{(0)}/d\tau = -P^{(0)2} \tag{19}$$

$$dP^{(1)}/d\tau = 0 \tag{20}$$

$$dP^{(2)}/d\tau = 2P^{(1)2} \tag{21}$$

where $\tau = tk_a p_o^{(0)}$. Equations 19–21 can be solved directly because they are independent of λ. It can be shown that the average particle size is a linear function of time and the limiting polydispersity is equal to 2 (McCoy and Madras, 1998).

For $\lambda = 0$ we employed a direct discretization technique to solve the PBE, Eq. 10. The domain of indefinite size $(0,\infty)$ was converted to a finite interval by the mapping function, $\xi = ay/(1-y)$, where $0 \le y \le 1$. This function guarantees that the grid is fine in the operating range of sizes and coarse at very high and very low sizes, where the number concentration of the particles is small. A finite difference scheme was applied to discretize the derivatives of the variables y and θ. The integrals in the PBE and the moments of the PBE were evaluated by Simpson's rule. The variable y was divided into 5,000 intervals, and the θ time step was set at 0.001. These values ensured stability and accuracy of the numeric scheme for solving the PBE and for calculating moments from the results.

The moment equations for $\lambda = 0$ are

$$dP^{(0)}/d\theta = P^{(0)} - \gamma P^{(0)2} \tag{22}$$

$$dP^{(1)}/d\theta = 0 \tag{23}$$

$$dP^{(2)}/d\theta = -(1/\sigma)P^{(2)} + 2\gamma P^{(1)2} \tag{24}$$

Equation 22 shows that breakage is first order and coalescence second order in particle number density for both particle mass and tracer mass. Equation 23 shows particle and tracer mass conservation. Equation 24 indicates that random ($\sigma = 3$) or midpoint fission ($\sigma = 2$) influences the second moment (McCoy and Madras, 1998). Equations 22–24 can be solved exactly for initial conditions, $P_o^{(0)} = P_o^{(1)} = 1$ and arbitrary $P_o^{(2)}$

$$P^{(0)}(\theta) = e^{\theta}/\left[1+\gamma(e^{\theta}-1)\right] \tag{25}$$

$$P^{(1)}(\theta) = P_o^{(1)} \tag{26}$$

$$P^{(2)}(\theta) = \left(P_o^{(2)} - 2\sigma\gamma\right)e^{-\theta/\sigma} + 2\sigma\gamma \tag{27}$$

$$P^{pd}(\theta) = P^{(0)}(\theta)P^{(2)}(\theta)/\left[P^{(1)}(\theta)\right]^2 = \left[\left(P_o^{(2)} - 2\sigma\gamma\right)e^{-\theta/\sigma} + 2\sigma\gamma\right]e^{\theta}/\left[1+\gamma(e^{\theta}-1)\right] \tag{27a}$$

Moments equations for TMD are identical, with C replacing P. The limits as $\theta \to \infty$ yield the stationary solutions, $P_{\text{eq}}^{(0)} = 1/\gamma$, $P_{\text{eq}}^{(1)} = P_o^{(1)}$, $P_{\text{eq}}^{(2)} = 2\sigma\gamma$, so, $P_{\text{eq}}^{\text{avg}} = \gamma$ and $P^{pd} = 2\sigma$. The

time dependences for C and P are different, however, because the initial conditions for second moments are in general different.

The time-dependent mixing entropy for the tracer distributed among the particles has the standard statistical definition (Reif, 1965)

$$S_{\mathrm{TMD}}(\theta) = s_{\mathrm{TMD}}(\theta)/R_g$$
$$= -\int_0^\infty \left[C(\zeta,\theta)/C^{(0)}(\theta)\right] \ln\left[C(\zeta,\theta)/C^{(0)}(\theta)\right] d\zeta \quad (28)$$

where S is entropy in units of the gas constant, R_g. A similar definition for $P(\xi,\theta)$ provides a measure of how entropy changes as particles aggregate and/or fragment,

$$S_{\mathrm{PSD}}(\theta) = -\int_0^\infty \left[P(\xi,\theta)/P^{(0)}(\theta)\right] \ln\left[P(\xi,\theta)/P^{(0)}(\theta)\right] d\xi \quad (29)$$

These expressions provide dimensionless entropy per particle, and are multiplied by $R_g p_o^{(0)} P^{(0)}(\theta)$ to obtain the total entropy of mixing. The difference of the entropies for the TMD and the PSD represents tracer mixing entropy relative to entropy for the same aggregation–fragmentation process without tracer

$$\Delta S = S_{\mathrm{TMD}} - S_{\mathrm{PSD}} \quad (30)$$

and serves as a measure of mixing.

Other measures of mixing can be defined by the relative polydispersity of the tracer and particle mass, for example

$$R_{pd} = C^{pd}(\theta)/P^{pd}(\theta) \quad (31)$$

which will approach unity as the tracer becomes evenly distributed among the particles. The polydispersity index is simply related to the variance as $P^{\mathrm{var}} = (P^{pd} - 1)P^{\mathrm{avg}\,2}$, so the ratio of variances, $C^{\mathrm{var}}(\theta)/P^{\mathrm{var}}(\theta)$, also shows the degree of mixing and approaches unity in a long time. These measures of mixing are easy to compute, as they involve only the three moments of the TMD and PSD.

The entropy expressions (Eqs. 28–30) require the full TMD and PSD, and, thus, need a numerical solution to the population balance equation. As we will demonstrate shortly, the PSD entropy change can be easily calculated for an exponential distribution, which is a similarity solution for reversible fragmentation–aggregation when $k_b \sim x^1$ and $k_a \sim x^0$ (McCoy and Madras, 1998). For more general solutions to the PBE, exact numerical solutions or moment approximations are needed to obtain expressions for $C(\zeta,\theta)$ and $P(\xi,\theta)$. Of course, particles in a stirred fluid are never at thermodynamic equilibrium as energy is added by the mixing mechanism, for example, through a rotating impeller. The energy effects of breakage and aggregation are usually significant, even in comparison to the substantial energy needed to sustain stirring in the fluid. The entropy is a measure of mixing, however, and shows the time evolution of mixing effectiveness. According to the present view, a stationary state can be reached by the particle-size and tracer distributions, and, thus, also by the mixing entropy. The stationary state is dynamic, with ongoing fragmentation and coalescence occurring along with the concomitant exchange of tracer molecules.

Exact Similarity Solution

The entropy evolution for reversible random fragmentation–aggregation when $k_b \sim x^1$ and $k_a \sim x^0$ (McCoy and Madras, 1998) can be exactly calculated for a system that always has a similarity solution, that is, an exponential distribution. In general for this case ($\lambda = 1$ in Eqs. 13–15), an arbitrary initial distribution evolves to the similarity form after a time that depends on the deviation of the initial distribution from an exponential form. McCoy and Madras (1998) showed that if the initial condition is exactly an exponential distribution, then the solution is always an exponential that can be written

$$P(\xi,\theta) = \left[P_o^{(1)}/\beta^2\right] \exp\left[-\xi/\beta\right] \quad (32)$$

The analogy with statistical mechanics is worth noting: in the canonical distribution the ratio of a particle's energy to the average thermal energy appears in the exponential (Reif, 1965), whereas in Eq. 32 it is the ratio of the particle mass to its average that appears. The moments for the similarity solution, Eq. 32, can all be simply represented as

$$P^{(j)} = P^{(0)}\beta^j j! \quad (33)$$

so that the polydispersity, $P^{pd}(\theta)$, is always 2 and the ratio of the first and zeroth moments is the average mass

$$P^{\mathrm{avg}}(\theta) = \beta \quad (34)$$

The distribution is, thus, governed by the average particle mass, $\beta(\theta)$, which satisfies the differential equation

$$d\beta/d\theta = -\beta^2 + \gamma \quad (35)$$

The proof given by McCoy and Madras (1998) demonstrated that the moments for Eq. 32 satisfy the moment equation (Eq. 12) for all j subject to β satisfying Eq. 35. An alternative proof is based on substituting Eq. 32 into the PBE (Eq. 11) and performing the integrations. The PBE becomes an equation with the coefficients of x^0 and x^1 satisfying Eq. 35 exactly. The exponential form of the solution, Eq. 32, is also compatible with an entropy maximization formalism (Jaynes, 1979; Englman, 1991; Denbigh and Denbigh, 1985) based on the method of Lagrange multipliers (Reif, 1965) applied to entropy defined by Eq. 29. Together with constraints represented by the zeroth and first moments, the maximization procedure yields Eq. 32. Only two constraints are required when $\lambda = 1$, because the moments are simply related to each other at all orders (Eq. 33). Other values for λ would require more constraints (in general, an infinite number of moments), and, thus, would not lead to the similarity form, Eq. 32. The PSD computed by the numerical solution of the PBE (Madras and McCoy, 2002), however, is frequently found to be nearly exponential, and, therefore, approximates self-similarity when

plotted either as the distribution or its cumulative integral. Therefore, as mixing entropy is influenced by the PSD evolution, the apparent self-similarity suggests that tracer mixing will not be strongly affected by the mass dependence of the fragmentation–aggregation rate coefficients.

With initial condition $\beta(\theta=0)=P_o^{(1)}/P_o^{(0)}=1$, the solution to Eq. 35 can be written in two equivalent forms

$$\beta(\theta)=\gamma^{1/2}\tanh\left[\theta\gamma^{1/2}+\tanh^{-1}\left(1/\gamma^{1/2}\right)\right]$$
$$=\left[(1+e^{2\theta\sqrt{\gamma}})\sqrt{\gamma}+(-1+e^{2\theta\sqrt{\gamma}})\gamma\right]/\left[(-1+e^{2\theta\sqrt{\gamma}})+(1+e^{2\theta\sqrt{\gamma}})\sqrt{\gamma}\right] \quad (36)$$

which have the long-time limit (McCoy and Madras, 1998)

$$\beta(\theta\to\infty)=\gamma^{1/2} \quad (37)$$

Equation 36 reduces to similarity expressions for $\gamma=0$ (fragmentation only; Ziff, 1991)

$$\beta(\theta)=1/(1+\theta) \quad (38)$$

and to first-order in θ for $\gamma\gg1$ (aggregation only; Friedlander and Wang, 1966)

$$\beta(\theta)=1+\gamma^{\theta} \quad (39)$$

The great advantage of Eq. 32 is its simplicity, permitting evaluation of evolving distributions for any value of γ (the ratio of fragmentation and aggregation rate coefficients) by straightforward calculation of β, the average particle mass.

By substituting Eq. 32 into Eq. 29 and utilizing Eq. 33 with integration over ξ, the expression for time-dependent en-

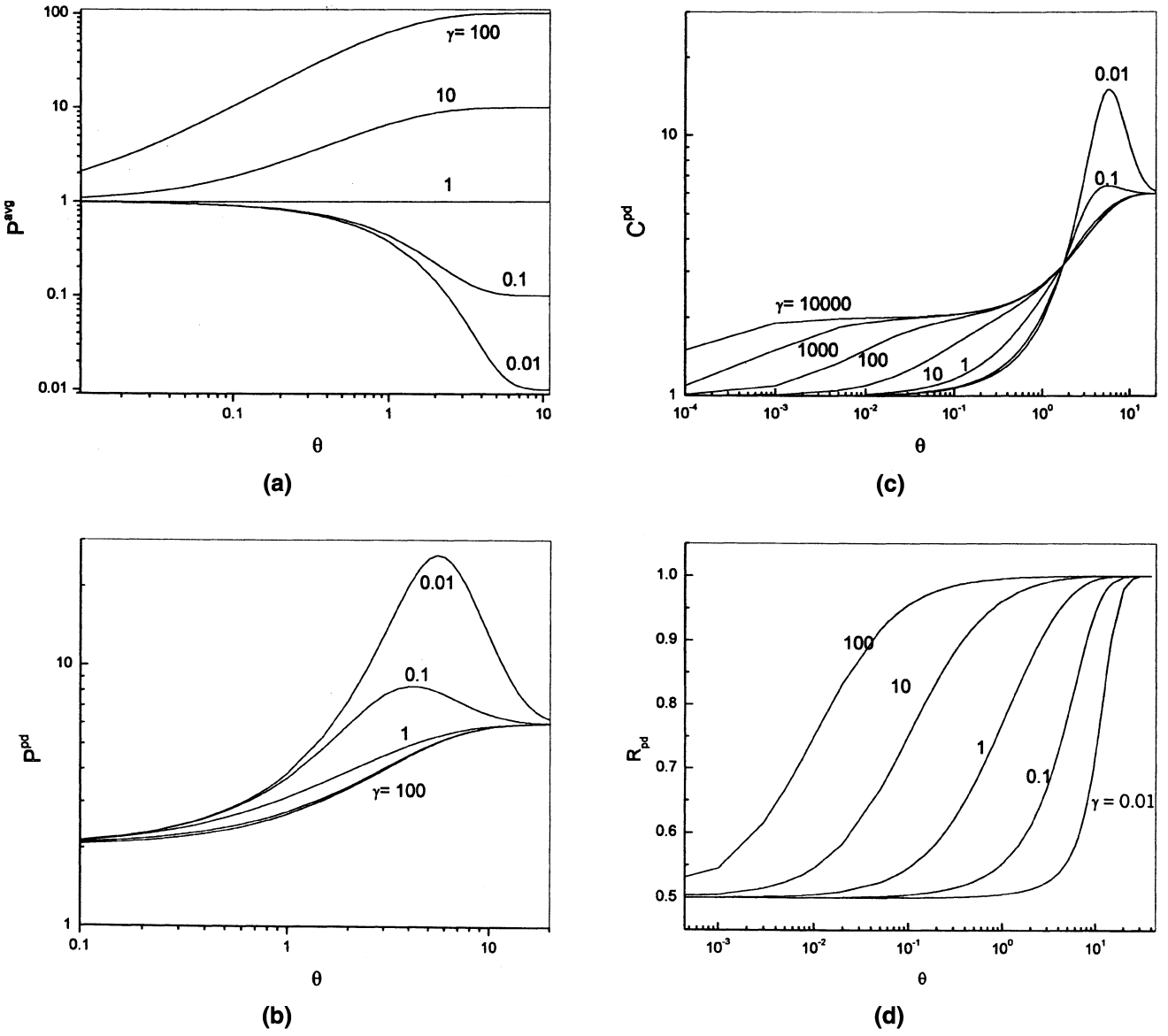

Figure 1. Time evolution of (a) PSD average mass, (b) PSD polydispersity, (c) TMD polydispersity, and (d) polydispersity mixing ratio, R_{pd}, for random fragmentation ($\sigma=3$), and $\lambda=0$.

tropy in units of R_g becomes simply

$$S(\theta) = 1 + \ln\ \beta(\theta) \tag{40}$$

so that the initial value is unity when $\beta_o = 1$. If we want dimensionless total entropy of all particles rather than entropy per mole of particles, we multiply Eq. 40 by $P^{(0)}(\theta) = \beta$. The scaled entropy production rate from Eqs. 40 and 35

$$dS/d\theta = \beta^{-1} d\beta/d\theta = (\gamma - \beta^2)/\beta \tag{41}$$

vanishes when the stationary state (Eq. 37) is reached. Although the TMD entropy calculation cannot be performed for $\lambda = 1$, the similarity solution provides a convenient comparison for the PSD dynamics.

Results and Discussion

Numerical computations were confirmed by numerically integrating the distributions according to definitions of the zeroth, first, and second moments (Eq. 11), and comparing to the solutions of the differential equations for moments (Eqs. 25–27). For all calculations, the agreement was accurate. Long time calculations were also checked by reducing the time interval of the numerical integration.

Results for the moments are plotted in Figure 1 for $\lambda = 0$, *random breakage* ($\sigma = 3$), and various values of γ. The initial condition is an exponential distribution, Eq. 32, with $\beta(\theta = 0) = 1$ and $P_o^{(1)} = 1$. The average dimensionless mass, $P^{\text{avg}}(\theta)$, reaches the limit γ at large times (Figure 1a). The polydispersity, $P^{pd}(\theta)$, for random fission ($\sigma = 3$ in Eq. 27) starts from its initial value 2 and approaches the value 6 at large times (Figure 1b). As already mentioned, $P^{pd} = 2$ is the similarity solution value (McCoy and Madras, 1998) when aggregation totally dominates ($\gamma \to \infty$). The polydispersity for TMD reaches a plateau at $C^{pd} = 2$ (Figure 1c) before approaching the final value of 6 for all γ. The ratio of polydispersity indices for TMD and PSD increase to unity for all values of γ (Figure 1d).

Polydispersity indices are plotted in Figure 2 for $\lambda = 0$, *midpoint breakage* ($\sigma = 2$), and various values of γ. Zeroth and first moments are not affected by the fragmentation stoichiometry, either random or midpoint, as already mentioned. Ottino et al. (2000) comment on conditions for breakage into two equal-size daughter droplets. For drops that are small relative to a criterion containing the critical capillary number, a two-dimensional extended flow causes a symmetric thinning (necking) of the connecting liquid. Although the conditions are constraining, the behavior is interesting as a limiting behavior.

For $\gamma < 1$, the polydispersity of both the PSD (Figure 2a) and the TMD (Figure 2b) increases to a maximum before declining to the limit value of 4. According to the definition following Eq. 3, for constant total mass of particles, polydispersity depends on the product of zeroth and second moments given by Eq. 27a. Owing to the different rates of change for the two moments when fragmentation dominates ($\gamma < 1$), the maximum polydispersity occurs, which is dependent on the initial conditions. The polydispersity ratio, however, increases monotonically to unity for all values of γ (Figure 2c)

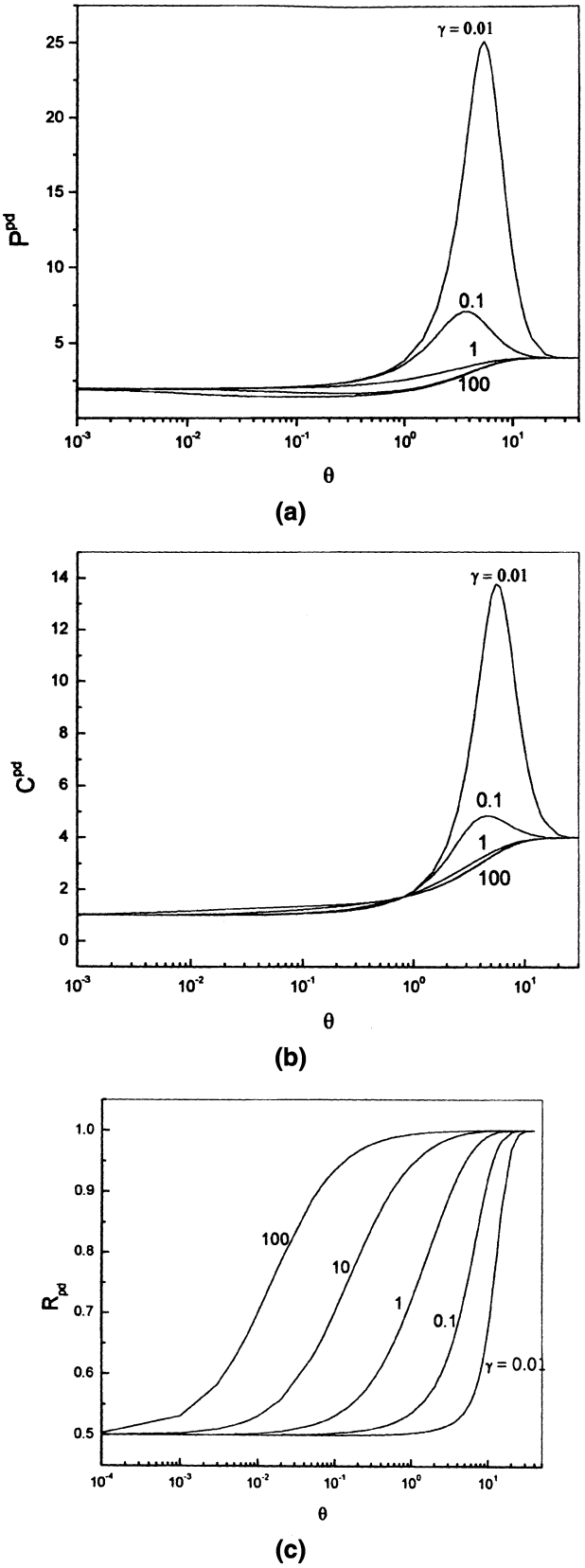

Figure 2. Time evolution of (a) PSD polydispersity, (b) TMD polydispersity, and (c) polydispersity mixing ratio, R_{pd}, for midpoint fragmentation ($\sigma = 2$), and $\lambda = 0$.

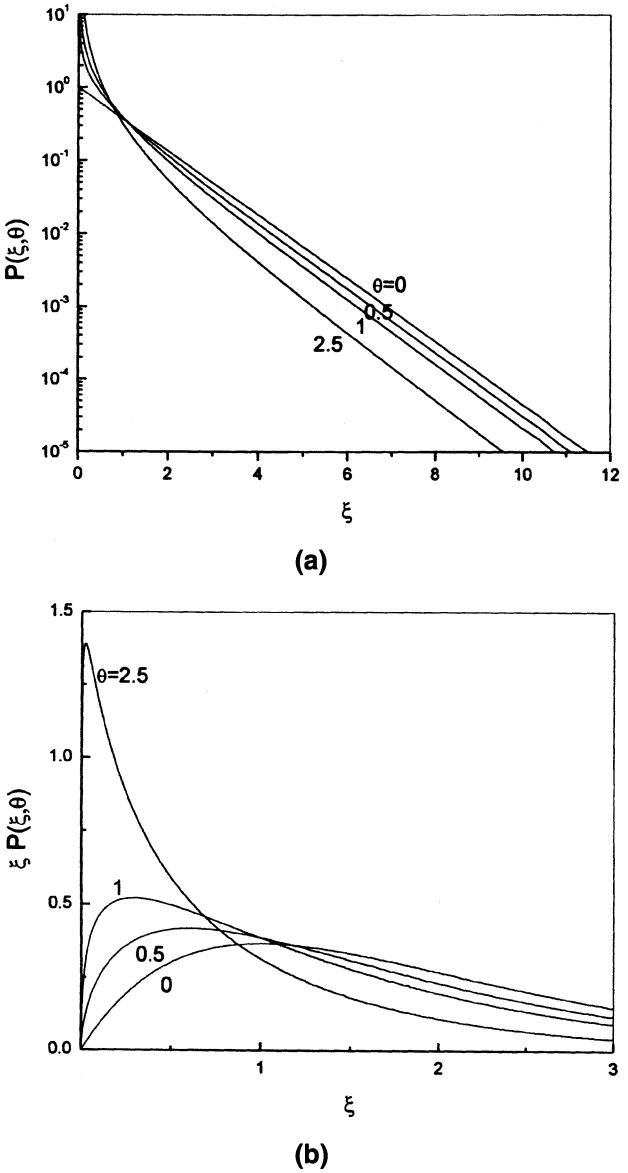

Figure 3. Time evolution of (a) number distribution and (b) mass distribution with exponential initial condition for $\lambda = 0$ and $\gamma = 0.01$.

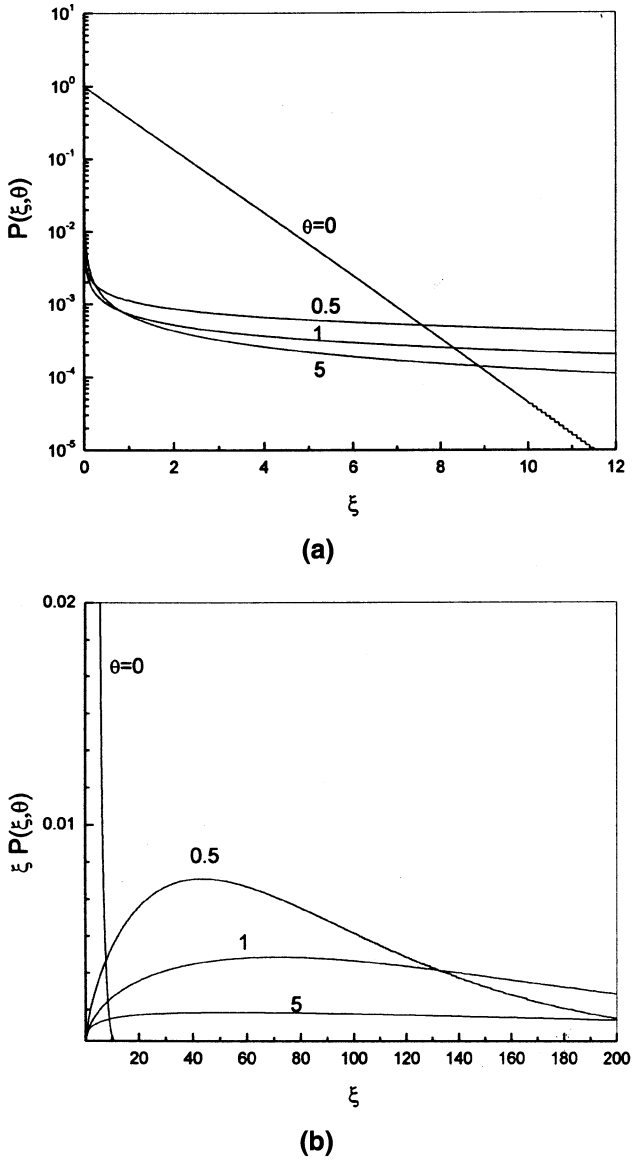

Figure 4. Time evolution of (a) number distribution and (b) mass distribution with exponential initial condition for $\lambda = 0$ and $\gamma = 100$.

as the tracer is completely mixed among the particles. These results agree with similar behavior shown in Figure 1 for random fragmentation.

Particle distributions are plotted in Figures 3 and 4 for $\gamma =$ 0.01 and 100, respectively, both (1) as (logarithm of) number distributions, and (2) as mass distributions. Initially, the distribution is exponential. Even though the PSDs are not exactly similarity solutions, they are at least partially linear on the semilog plots, suggesting why the self-similar approximation attributed to experimental data is frequently inferred.

When the initial condition for the TMD is a Dirac delta distribution positioned at $\zeta = 1$, $C(\zeta, \theta = 0) = \delta(\zeta - 1)$, the identical-size particles fragment and aggregate, causing the distribution to broaden. Figure 5 shows such broadening for the mass distribution when $\gamma = 1$. At time $\theta = 1$ small peaks at $\zeta = 2$, 3, and 4 are evident and are caused by aggregation of particles of mass $\zeta = 1$. The polydispersity mixing ratio shows the evolution to unity for complete mixing of the tracer, similar to Figures 1d and 2c.

The entropy change with time for $\lambda = 0$ is plotted in Figure 6. The TMD entropy increases during small values of time for all γ as the tracer is mixed throughout the particles (Figure 6a). At some point, however, the fragmentation or aggregation of particles, which causes entropy to decrease (Figure 6b), overwhelms the tracer effect, and entropy begins to decline. The entropy difference between TMD and PSD (Figure 6c) increases monotonically to its stationary state value.

Similarity solution

All the similarity solution results (for $\lambda = 1$ and random fission) illustrate the PSD behavior with an initial exponential distribution (polydispersity of two). The evolution of the

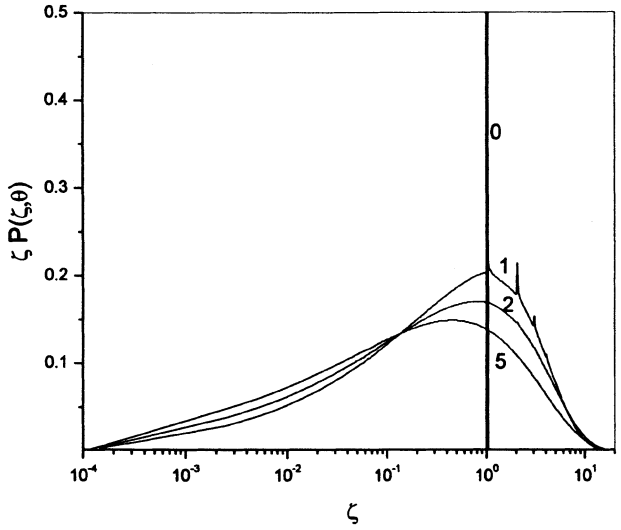

Figure 5. Time evolution of mass distribution with delta distribution initial condition for $\lambda = 0$ and $\gamma = 1$.

zeroth moment (Eq. 33), $P^{(0)}(\theta) = 1/\beta$, second moment, $P^{(2)}(\theta) = 2\beta$, and average mass, $P^{\text{avg}}(\theta) = \beta$, are plotted in Figure 7 by evaluating Eq. 36 for $\beta_o = 1$ and values of γ ranging from 0.01 (dominated by fragmentation) to 100 (dominated by aggregation). The average mass either increases or decreases depending on whether aggregation or fragmentation dominates. If $\gamma = 1$, $\beta(\theta) = 1$ is constant with time and serves as the dividing line between dominance of aggregation or fragmentation. Stationary states (long-time asymptotes) are given by $\beta = \gamma^{1/2}$. Because the polydispersity ($= 2$) and the first moment ($= 1$) are invariant in time, the second moment is always twice the average mass.

Figure 8 shows the self-similar evolution of an initially exponential distribution, $\beta(\theta = 0) = 1$, for fragmenting particles, $\gamma = 0.01$. Also plotted is the mass distribution, defined by $\xi P(\xi,\theta)d\xi$ and representing the mass of particles in the interval $(\xi,\ \xi + d\xi)$. At the longest times, the mass distribution becomes steeper and narrower as it evolves to a delta distribution located at $\xi = 0$. Figure 9 for aggregating particles, $\gamma = 100$, shows the evolving distributions becoming broader and shallower with time. The agreement with Figures 3 and 4 for the case $\lambda = 0$ is obvious.

In Figure 7d the entropy time dependence (Eq. 40) is plotted for several values of γ. When aggregation dominates ($\gamma > 1$), entropy per particle increases as fluid elements are mixed into fewer particles. When fragmentation dominates ($\gamma < 1$), the entropy per particle decreases because fluid elements are separated into a larger number of particles. When $\gamma = 1$, the number of particles does not change. The total PSD entropy for both aggregation and fragmentation decreases because of division by increasing β, which follows from Eq. 40 and the definition of S_{tot}

$$S_{\text{tot}}(\theta) = P^{(0)}(\theta)S(\theta) = [1 + \ln\ \beta(\theta)]/\beta \qquad (42)$$

Because the entropy of the turbulent fluid increases much more than the entropy for the particles decreases, the en-

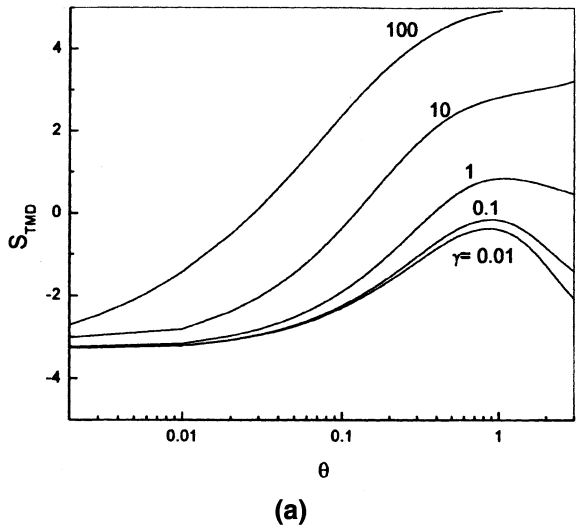

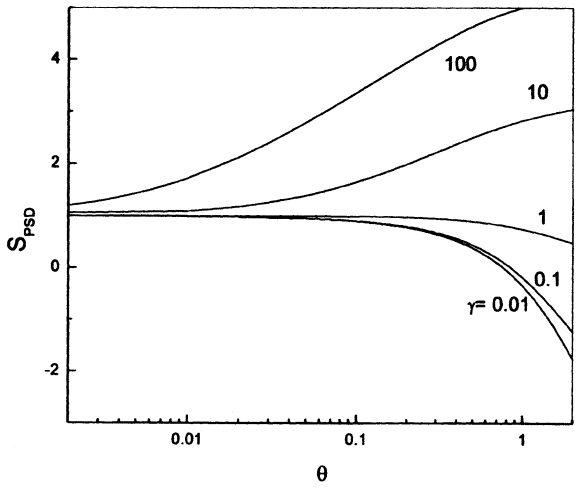

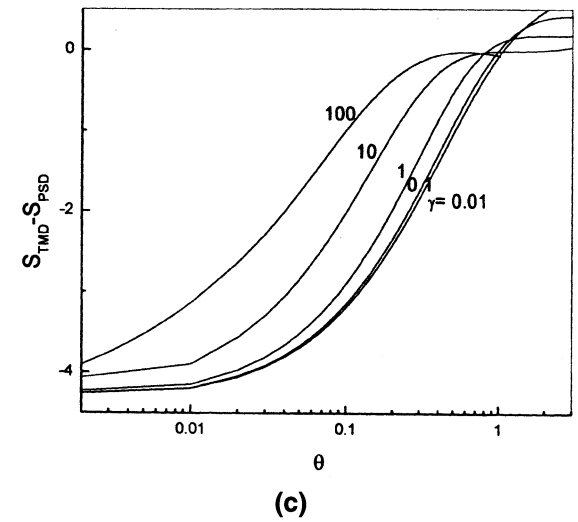

Figure 6. Entropy per particle (in units of R_g) versus scaled time ($\lambda = 0$) for (a) TMD, for (b) PSD, and (c) for the difference.

tropy of the entire system (particles plus turbulent fluid) increases overall due to the energy input. The Second Law of Thermodynamics is, thus, satisfied. An analogy with gas compression may be helpful in understanding the entropy decrease of particles alone. The molar entropy of an isothermal ideal gas process varies with pressure p according to $dS = -R_g d \ln p$, so that compression decreases the gas entropy, even as the entropy of the gas surroundings increases.

Conclusion

As in most studies of dynamic systems, we wish to describe mathematically how a fragmentation–aggregation system evolves (relaxes) to stationary states. Because the fundamental variable is the particle-size distribution, fragmentation–aggregation dynamics are distinct from typical transport and reaction relaxation kinetics, which focus on local thermodynamic properties such as temperature, concentration, or kinetic energy (fluid velocity). Other systems that fall into the category of distribution kinetics are polymerization and depolymerization, crystal growth and dissolution, and microbial propagation and growth. In all these cases, moments of the property size (such as with respect to particle mass) represent observable quantities. In this and other work we have directed our attention to spatially homogeneous systems (the treatment of the steady-state plug-flow tubular reactor is merely a transformation of time for the batch reactor to distance over axial velocity). The governing equation is the PBE, an integrodifferential equation that gives rise to a hierarchy of ordinary differential equations for moments of increasing order. The rate coefficients for the PBE embody all the system characteristics, such as operating, geometric, and fluid properties, pertaining to the dynamics. Details of the aggregation–fragmentation processes, including the mechanics of

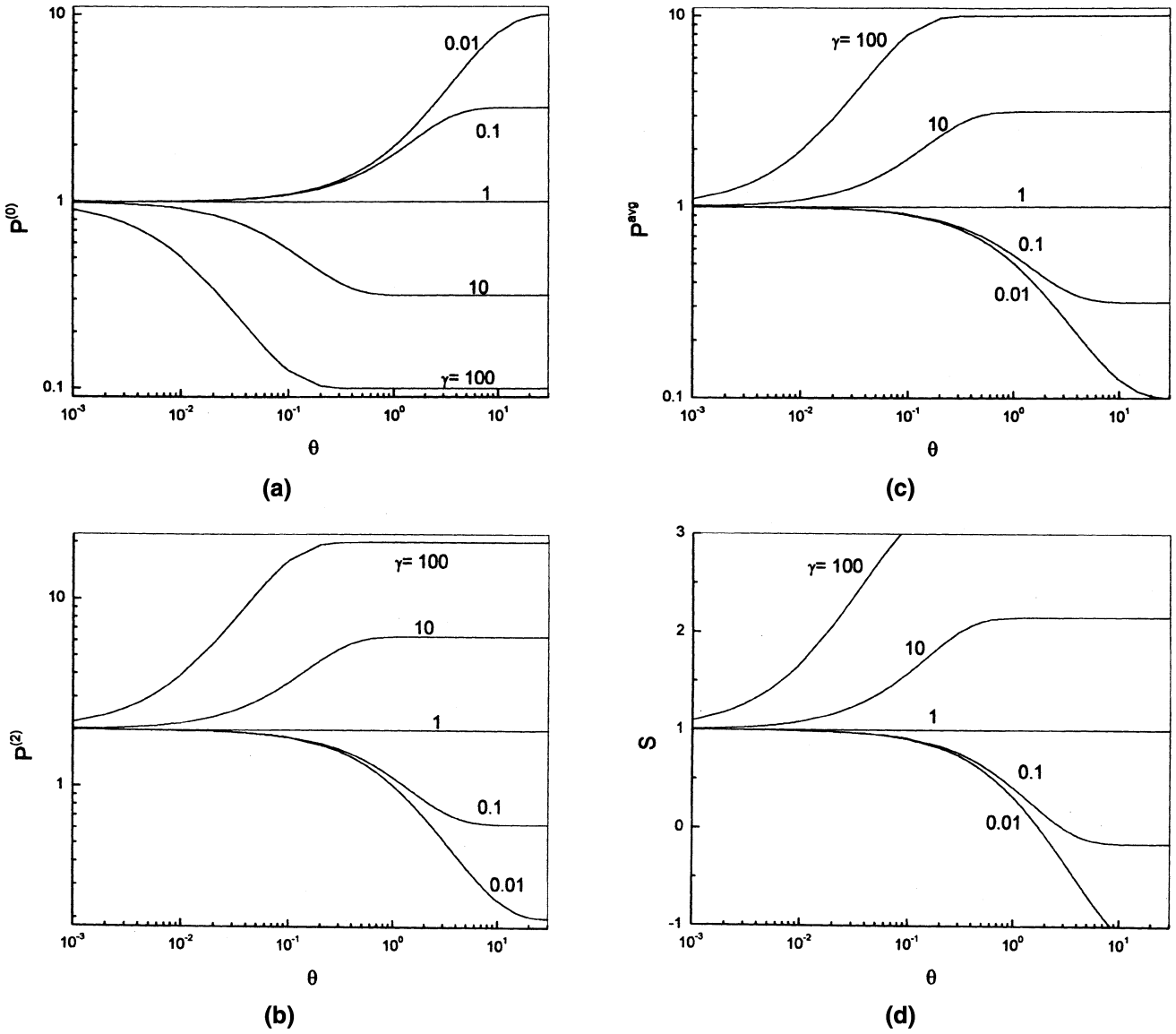

Figure 7. Time evolution of (a) zeroth, (b) second moments, (c) average mass vs. time, and (d) entropy per particle ($\lambda = 1$, $\beta_o = 1$); stationary states (long-time asymptotes) are given by $\beta \to \gamma^{1/2}$.

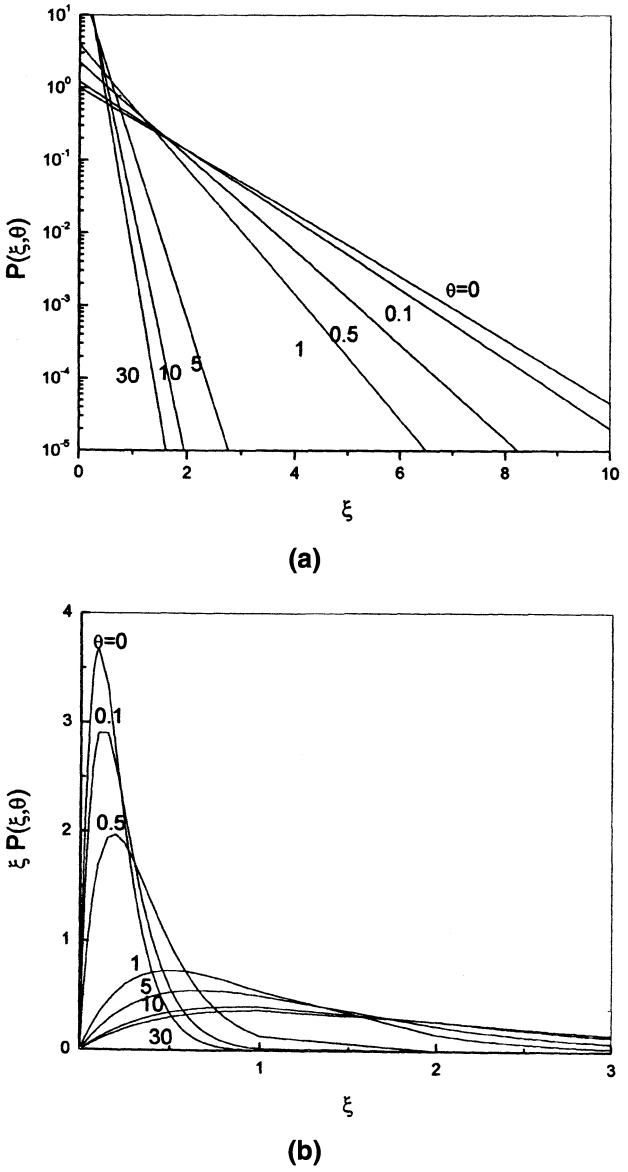

Figure 8. Time evolution of (a) number distribution and (b) mass distribution for $\lambda = 1$, $\beta_o = 1$, and $\gamma = 0.01$.

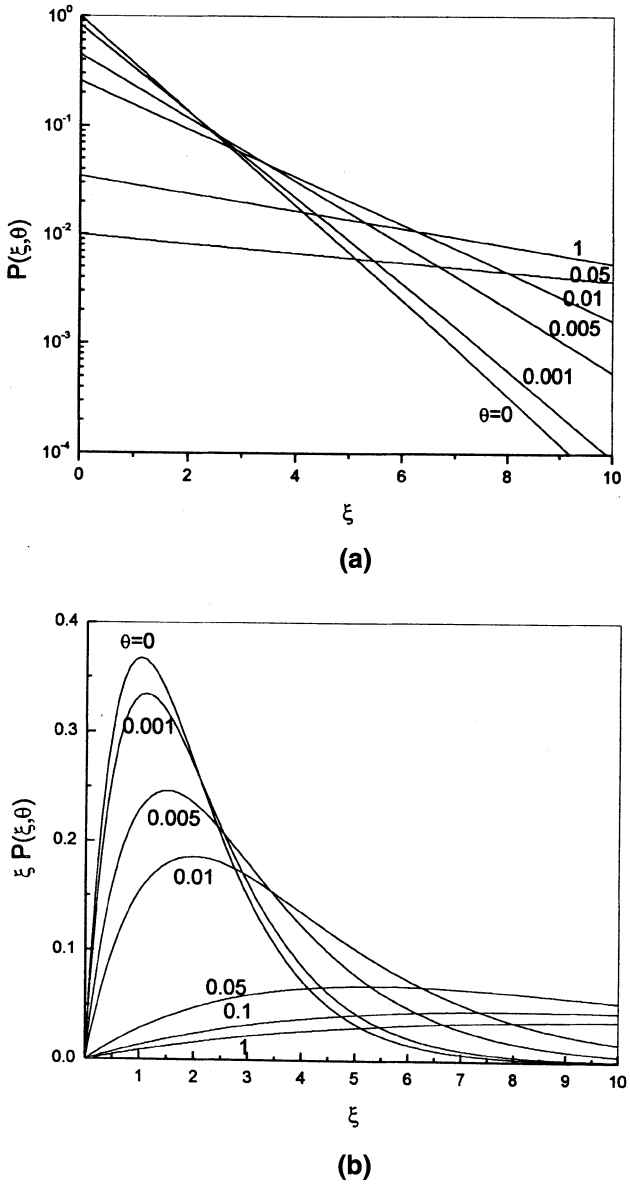

Figure 9. Time evolution of (a) number distribution and (b) mass distribution for $\lambda = 1$, $\beta_o = 1$, and $\gamma = 100$.

viscous, inertial, interfacial, deformation, and thermal effects, are incorporated into the rate coefficients.

Our approach illustrates how tracer mixing in aggregation–fragmentation processes is based on the governing population balance equation for the continuous particle-size and tracer-concentration distributions. The PBEs can be solved either by moment methods (for special cases) or in general by numerical techniques. One special case ($\lambda = 1$) has an exact similarity solution, although many solutions approximate self-similarity, in particular, the case $\lambda = 0$ treated here. The similarity solution provides a simple comparison computation for the evolving particle-size distribution. The degree of mixing can be represented by the difference of the entropy of the TMD and of the PSD, which increases to a stationary-state value for different levels of concurrent aggregation and fragmentation. Simpler measures of mixing are based on ratios of the second moments (variance or polydispersity) of the TMD and PSD. The computations yield results for an idealized model system that can be readily solved, providing information that can guide more general attempts to understand mixing in dispersed, turbulent systems.

Acknowledgment

This work was supported in part by NSF Grant CTS-9810194.

Literature Cited

Aizenman, M., and T. A. Bak, "System of Reacting Polymers," *Commun. Math. Phys.*, **65**, 203 (1979).

Chatzi, E. G., and C. Kiparissides, "Steady-State Drop-Size Distributions in High Holdup Fraction Dispersion Systems," *AIChE J.*, **41**, 1640 (1995).

Church, J. M., and R. Shinnar, "Stabilizing Liquid-Liquid Dispersions by Agitation," *Ind. Eng. Chem.*, **53**, 479 (1961).
Cohen, R. D., "The Self-Similar Cluster Size Distribution in Random Coagulation and Breakup," *J. Colloid Interface Sci.*, **149**, 261 (1992).
Coulaloglou, C. A., and L. L. Tavlarides, "Description of Interaction Processes in Agitated Liquid-Liquid Dispersions," *Chem. Eng. Sci.*, **32**, 1289 (1977).
Denbigh, K. G., and J. S. Denbigh, *Entropy in Relation to Incomplete Knowledge*, Cambridge University Press, Cambridge, p. 105 (1985).
Englman, R., "Fragments of Matter from a Maximum-Entropy Viewpoint," *J. Phys. Condens. Matter*, **3**, 1019 (1991).
Family, F., P. Meakin, and J. M. Deutch, "Kinetics of Coagulation with Fragmentation: Scaling Behavior and Fluctuations," *Phys. Rev. Lett.*, **57**, 727 (1986).
Friedlander, S. K., and C. S. Wang, "The Self-Preserving Particle Size Distribution for Coagulation by Brownian Motion," *J. Colloid Interface Sci.*, **22**, 126 (1966).
Goren, S. L., "Distribution of Lengths in the Breakage of Fibres or Linear Polymers," *Can. J. Chem. Eng.*, **46**, 105 (1968).
Hounslow, M. J., J. M. K. Pearson, and T. Instone, "Tracer Studies of High-Shear Granulation: II. Population Balance Modeling," *AIChE. J.*, **47**, 1984 (2001).
Ilievski, D., and E. T. White, "Agglomeration During Precipitation: I. Tracer Crystals for $Al(OH)_3$ Precipitation," *AIChE. J.*, **41**, 518 (1995).
Jaynes, E. T., *The Maximum Entropy Formalism*, R. D. Levine and M. Tribus, eds., MIT Press, Cambridge, MA (1979).
Kostoglou, M., and A. J. Karabelas, "A Contribution Towards Predicting the Evolution of Droplet Size Distribution in Flowing Dilute Liquid/Liquid Dispersions," *Chem. Eng. Sci.*, **56**, 4283 (2001).
Lam, A., A. N. Sathyagal, S. Kumar, and D. Ramkrishna, "Maximum Stable Drop Diameter in Stirred Dispersions," *AIChE J.*, **42**, 1547 (1996).
Madras, G., and B. J. McCoy, "Time Evolution of Molecular Weight Distributions for Ultrasonic Degradation of Polymers," *AIChE J.*, **47**, 2341 (2001).
Madras, G., and B. J. McCoy, "Numerical and Similarity Solutions for Reversible Population Balance Equations With Size-Dependent Rates," *J. Colloid Interface Sci.*, **246**, 356 (2002).
McCoy, B. J., and G. Madras, "Evolution to Similarity Solutions for Fragmentation and Aggregation," *J. Colloid Interface Sci.*, **201**, 200 (1998).
McCoy, B. J., and M. Wang, "Continuous-Mixture Fragmentation Kinetics: Particle Size Reduction and Molecular Cracking," *Chem. Eng. Sci.*, **49**, 3773 (1994).
Muzzio, F. J., M. Tjahjadi, and J. M. Ottino, "Self-Similar Drop-Size Distributions Produced by Breakup in Chaotic Flows," *Phys. Rev. Lett.*, **67**, 54 (1991).
Ottino, J. M., F. J. Muzzio, M. Tjahjadi, J. G. Franjione, S. C. Jana, and H. A. Kusch, "Chaos, Symmetry, and Self-Similarity: Exploiting Order and Disorder in Mixing Processes," *Science*, **257**, 754 (1992).
Ottino, J. M., P. DeRoussel, S. Hansen, and D. V. Khakhar, "Mixing and Dispersion of Viscous Liquids and Powdered Solids," *Adv. Chem. Eng.*, **25**, 1 (2000).
Pearson, J. M. K., M. J. Hounslow, and T. Instone, "Tracer Studies of High-Shear Granulation: I. Experimental Results," *AIChE. J.*, **47**, 1978 (2001).
Prince, M. J., and H. W. Blanch, "Bubble Coalescence and Break-Up in Air-Sparged Bubble Columns," *AIChE J.*, **36**, 1485 (1990).
Ramkrishna, D., *Population Balances—Theory and Application to Particulate Systems in Engineering*, Academic Press, San Diego, CA (2000).
Reif, F., *Fundamentals of Statistical and Thermal Physics*, McGraw-Hill, New York (1965).
Spicer, P. T., and S. E. Pratsinis, "Coagulation and Fragmentation: Universal Steady-State Particle-Size Distribution," *AIChE J.*, **42**, 1612 (1996).
Sundaresan, S., "Modeling the Hydrodynamics of Multiphase Flow Reactors: Current Status and Challenges," *AIChE J.*, **46**, 1102 (2000).
Valentas, K. J., and N. R. Amundson, "Breakage and Coalescence in Dispersed Phase Systems," *Ind. Eng. Chem. Funds.*, **5**, 533 (1966).
Weidenbaum, S. S., "Mixing of Solids," *Adv. Chem. Eng.*, **2**, 209, (1958).
Ziff, R. M., "New Solutions to the Fragmentation Equation," *J. Phys. A: Math. Gen.*, **24**, 2821 (1991).

Manuscript received Oct. 24, 2001, and revision received Mar. 18, 2002.